Please cite this article as: Mondragón-Rodríguez *et. al.*, (2020). Hippocampal Unicellular Recordings and Hippocampal-dependent Innate Behaviors in an Adolescent Mouse Model of Alzheimer's disease,*Bio-protocol* 10 (4): e3529. DOI: 10.21769/BioProtoc.3529.

bio-protocol www.bio-protocol.org/e3529 Bio-protocol 10(04): e3529. DOI:10.21769/BioProtoc.3529

Hippocampal Unicellular Recordings and Hippocampal-dependent Innate Behaviors in an Adolescent Mouse Model of Alzheimer's disease

Siddhartha Mondragón-Rodríguez[1, 2, *], Benito Ordaz[2], Erika Orta-Salazar[2], Sofia Díaz-Cintra[2], Fernando Peña-Ortega[2] and George Perry[3]

[1]National Council for Science and Technology (CONACYT), México, México; [2]Developmental Neurobiology and Neurophysiology, Institute of Neurobiology, National Autonomous University of México (UNAM), Querétaro, México; [3]Neuroscience Institute and Department of Biology, College of Sciences, University of Texas at San Antonio (UTSA), San Antonio, Texas

*For correspondence: sidmonrod@gmail.com

[Abstract] Transgenic mice have been used to make valuable contributions to the field of neuroscience and model neurological diseases. The simultaneous functional analysis of hippocampal cell activity combined with hippocampal dependent innate task evaluations provides a reliable experimental approach to detect fine changes during early phases of neurodegeneration. To this aim, we used a merge of patch-clamp with two hippocampal innate behavior tasks. With this experimental approach, whole-cell recordings of CA1 pyramidal cells, combined with hippocampal-dependent innate behaviors, have been crucial for evaluating the early mechanism of neurodegeneration and its consequences. Here, we present our protocol for *ex vivo* whole-cell recordings of CA1 pyramidal cells and hippocampal dependent innate behaviors in an adolescent (p30) mice.

Keywords: Patch-clamp, Innate behavior, Neurodegeneration, Hippocampus, Pyramidal cells, Subthreshold oscillations and Alzheimer's disease

[Background] Transgenic mice have been widely used to study the cellular and behavioral alterations underlying complex brain disorders, such as Alzheimer's Disease (AD) (Mahar *et al*., 2017; Mondragón-Rodríguez *et al*., 2018a, 2018b and 2019). The current and most accepted hypothesis regarding AD pathophysiology upholds that accumulation of amyloid-β (Aβ) lead to neurotoxicity and abnormally phosphorylated tau (pTau) in the hippocampus (Ittner *et al.*, 2010). Additionally, several studies have suggested that protein aggregation correlates with cell damage and the cognitive deficits that characterize AD development (Selkoe, 1990; Oddo *et al*., 2003; LaFerla *et al*., 2007; Ittner *et al.*, 2010; Mondragón-Rodríguez *et al*., 2014). However, there is evidence demonstrating that Ca^{2+} dysregulation due to presenilin (PS) mutation occurs prior to the formation of Aβ plaques and pTau accumulation (review in Tong *et al*., 2018; Hashimoto *et al*., 2018). Thus, electrophysiological data demonstrated that the PS holoprotein itself functions as a passive ER Ca^{2+} leak channel that is impaired in mutant PS leading to Ca^{2+} overload (review in Tong *et al*., 2018; Hashimoto *et al*., 2018). Of relevance, the activities of the major kinases involved in tau phosphorylation are Ca^{2+} dependent (review in Tong *et al*., 2018). PS is ubiquitously found in cellular membranes, including the ER membrane (review in Tong *et al*., 2018; Hashimoto *et al*., 2018). PS mutation disrupts ER Ca^{2+} release through inositol 1,4,5-triphosphate

Please cite this article as: Mondragón-Rodríguez *et. al.*, (2020). Hippocampal Unicellular Recordings and Hippocampal-dependent Innate Behaviors in an Adolescent Mouse Model of Alzheimer's disease,*Bio-protocol* 10 (4): e3529. DOI: 10.21769/BioProtoc.3529.

receptors ($InsP_3R$) and ryanodine receptors (RyR) that elevate cytoplasmic Ca^{2+}, therefore, affecting synaptic transmission and brain activity (review in Tong *et al*., 2018; Hashimoto *et al*., 2018). Furthermore, recent evidence suggests that changes in brain activity, potentially leading to hippocampal memory alterations, occurs before any clear neurodegenerative signs appear (Mucke and Selkoe., 2012; Peña-Ortega *et al*., 2012; Mondragón-Rodríguez *et al*., 2013, 2017, 2018a and 2018b). In this regard, we have reported that brain activity self-generated in the hippocampus is affected before the detection of cognitive dysfunctions (Mondragón-Rodríguez *et al*., 2018a, 2018b and 2019). Specifically, we found that CA1 pyramidal neurons from an adolescent transgenic mouse model showed less spike accommodation and increased subthreshold membrane oscillations (Mondragón-Rodríguez *et al*., 2018a).

To achieve these findings, patch-clamp recordings of pyramidal cells were performed (first group), and hippocampal dependent innate behaviors were assessed in a p30 (postnatal day 30) transgenic AD mouse model (second group) (Oddo *et al*., 2003).

To evaluate how pyramidal cells are challenged during the early stages of AD development, we performed electrophysiological analyses of their intrinsic properties (Mondragón-Rodríguez *et al*., 2018a). Action potential properties were examined using depolarizing current steps of increasing amplitude. Additionally, subthreshold oscillations in pyramidal cells, which are the main constituents of subthreshold-level activity (Peña *et al*., 2010; V-Ghaffari *et al*., 2016) were evaluated.

To address the cognitive state (hippocampal-dependent function) of p30 transgenic mice we performed burrowing and nesting tests (Salgado-Puga *et al*., 2015; Gjendal *et al*., 2019). While, typical hippocampal-dependent tests, such as the morris water maze, are not reliable in p30 mice, burrowing and nesting are examples of highly motivated innate behaviors in rodents (Deacon, 2012; Salgado-Puga *et al*., 2015). Additionally, both paradigms have proven to be a reliable assay for monitoring the development of brain diseases in mice (Deacon *et al*., 2001; Orta-Salazar *et al*., 2013; Salgado-Puga *et al*., 2015). Thus, deterioration in the ability to perform activities of daily living is an early sign of AD development (Lilamand *et al*., 2019). Although several protocols exist in the literature, here we simplify and explain the procedures used by our research group with a well-defined scoring system applicable to p30 mice.

Materials and Reagents

Materials

A. Behavioral tasks

Nesting

1. Cotton square (5 cm x 5 cm, any commercial brand)

Burrowing

2. Handmade plastic black tube 20 cm long and 7.5 cm in diameter (The open end of the tube was elevated 2.5 cm from the floor (using two screws), to prevent accidental displacement of the

Please cite this article as: Mondragón-Rodríguez *et. al.*, (2020). Hippocampal Unicellular Recordings and Hippocampal-dependent Innate Behaviors in an Adolescent Mouse Model of Alzheimer's disease,*Bio-protocol* 10 (4): e3529. DOI: 10.21769/BioProtoc.3529.

tube's content. The opposite end of the tube was blocked and touched the floor, as shown in Figure 1)

Figure 1. Homemade plastic black tube used as a burrow

B. Electrophysiology

1. Plastic tubing for perfusion system (Tubing Master Flex, catalog number: 065009-16; Tygon E-3603 and Tygon tubing, Cole Parmer, catalog number: 06460-34)
2. Recording chamber and platform (Homemade, see Figure 8)
3. Capillary glass tubing (Borosilicate standard wall with filament, length = 10 cm, Warner Instruments, catalog number: G150F-4)
4. Camera with monitor (DAGE-MTI, catalog number: CCD-100)
5. Double edge razor blades (Any commercial brand)

Reagents

1. Na_2ATP (Sigma-Aldrich, catalog number: 34369078)
2. LiGTP (Sigma-Aldrich, catalog number: 85737048)
3. Potassium gluconic acid (Sigma-Aldrich, catalog number: 299274)
4. EGTA (Sigma-Aldrich, catalog number: 67425)
5. HEPES (Sigma-Aldrich, catalog number: 7365459)
6. Sucrose (Sigma-Aldrich, catalog number: S9378)
7. Potassium chloride (KCl) (Sigma-Aldrich, catalog number: P4504)
8. Sodium chloride (NaCl) (Sigma-Aldrich, catalog number: S9625)
9. Magnesium chloride ($MgCl_2$) (Sigma-Aldrich, catalog number: M8266)
10. Sodium bicarbonate ($NaHCO_3$) (Sigma-Aldrich, catalog number: S8875)
11. Calcium chloride ($CaCl_2$) (Sigma-Aldrich, catalog number: C3881)
12. D-glucose (Sigma-Aldrich, catalog number: D8270)
13. Cyanoacrylate (Any commercial brand)
14. Pentobarbital
15. Intracellular solution for patch-clamp recordings (see Recipes)
16. External solution (artificial cerebrospinal fluid (aCSF)) (see Recipes)
17. Internal solution (see Recipes)

Equipment

A. Behavioral tasks

Nesting

1. Individual cage (26 cm x 48 cm x 20 cm) with wood chip bedding

Burrowing

2. Individual cage (26 cm x 48 cm x 20 cm) with wood chip bedding

B. Electrophysiology

1. Peristaltic pump (DYNAMAX, model: Rp-1)
2. In line solution heater (Automatic Temperature Control, Warner Instruments, model: TC-324C)
3. Temperature controller (Harvard Apparatus, model: TC-202A)
4. Amplifier (Axon Instruments, model: Axo-clamp 2B amplifier)
5. Connector block (National Instruments, model: BNC-2110)
6. Digitizer (National Instruments, Digidata BNC-2110)
7. Micromanipulator (Sutter Instrument Co, model: MP-225)
8. Air table serial #119564, TMC and Faraday Cage (Homemade)
9. Microscope (NIKON, model: E600-FN)
10. Flaming/Brown Micropipette (Sutter Instrument Co, model: P-97)
11. Vibratome (Thermo Scientific, model: Microm HM-650V)

Software

1. Any available software that controls amplifier and digitizer, for example, pCLAMP™ Software. In our experiments we used software developed in LabView, National Instruments

Procedure

A. Behavioral tasks (both protocols are performed in the same behavioral room and all animals perform both tasks)

Nesting

1. Start the nesting protocol at 08:00 a.m., one hour before the dark phase (12-h light/12-h dark cycle). Place the animal into an individual cage filled only with wood-chip bedding (around 2 cm). After 60 min, place a cotton square (5 cm x 5 cm) on the bedding (Figure 2, see corner of the cage). Innately, animals use the cotton to build a nest. The following morning (08:00 a.m.), perform evaluation of nest.

Please cite this article as: Mondragón-Rodríguez *et. al.*, (2020). Hippocampal Unicellular Recordings and Hippocampal-dependent Innate Behaviors in an Adolescent Mouse Model of Alzheimer's disease,*Bio-protocol* 10 (4): e3529. DOI: 10.21769/BioProtoc.3529.

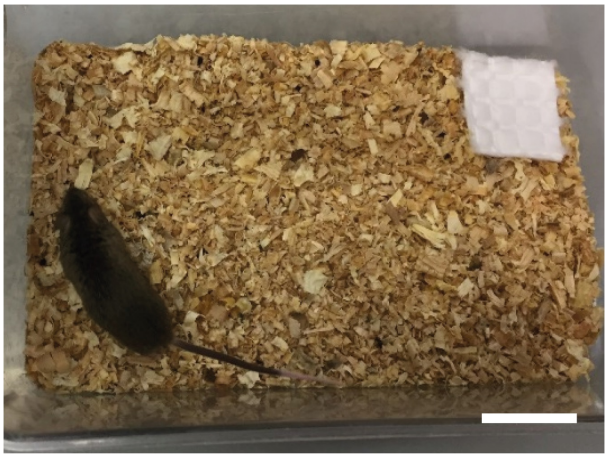

Figure 2. Place an animal in an individual cage with wood-chip bedding following by a cotton square 60 min later (scale bar = 5 cm)

Burrowing

1. Place each animal in an individual cage (26 cm x 48 cm x 20 cm) with the burrow tube filled up with 200 g of food pellets (these pellets are standard mouse food pellets normally supplied as their diet). The animals have access to water, but no access to food other than the one placed in the tube.
2. Start the test at 06:00 a.m., three hours before the dark phase. Record the amount of food pellets displaced after the first 2 h of the test.
3. The weight of the pellets burrowed for 2 h is then quantify by subtracting it from the original 200 g. The burrow tube is refill with pellets, and the test continue. Perform the final quantification of the displaced pellet weight after 12 h, as shown in figure 3.

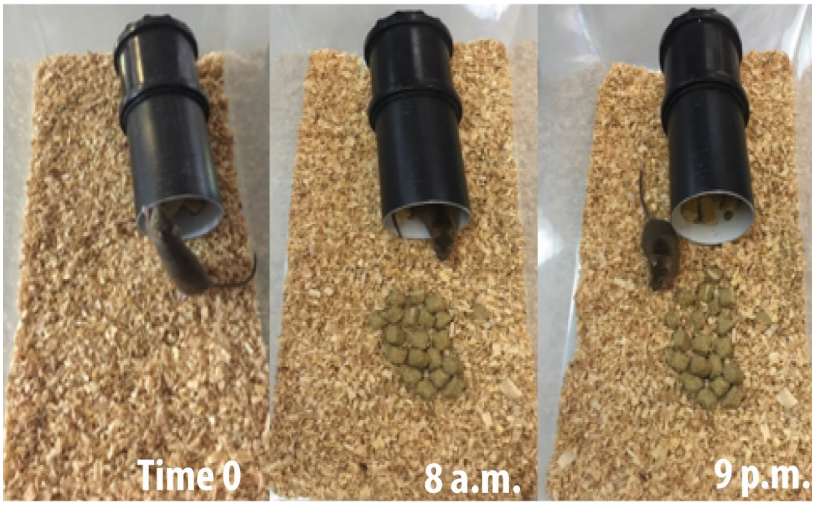

Figure 3. Plastic black tube with pellets displaced at time 0, 8 a.m. and 9 p.m.

Please cite this article as: Mondragón-Rodríguez *et. al.*, (2020). Hippocampal Unicellular Recordings and Hippocampal-dependent Innate Behaviors in an Adolescent Mouse Model of Alzheimer's disease,*Bio-protocol* 10 (4): e3529. DOI: 10.21769/BioProtoc.3529.

B. Electrophysiology

Patch-clamp (ethics approval should be obtained)

1. Deeply anesthetize the animals with pentobarbital (63 mg/kg, alternatives ketamine and xylazin) to perform an intravascular perfusion (30 ml) of modified aCSF bubbled with carbogen (95% O_2 and 5% CO_2). At the end of the infusion, decapitate the animal and remove the brain in ice-cold aCSF. To obtain para-sagittal slices (Figures 4 and 5), remove the cerebellum and brainstem, separate the brain hemispheres and glue them by their medial portion at a 30° angle (Figures 4 and 5). First, glue the brain to a piece of filter paper and then, glue the filter paper (with the brain) to the agar block (Figures 4 and 5, agar size tends to vary according to brain size). Throughout this process, the brain tissue should be immersed in normal aCSF with continuous bubbled with carbogen.

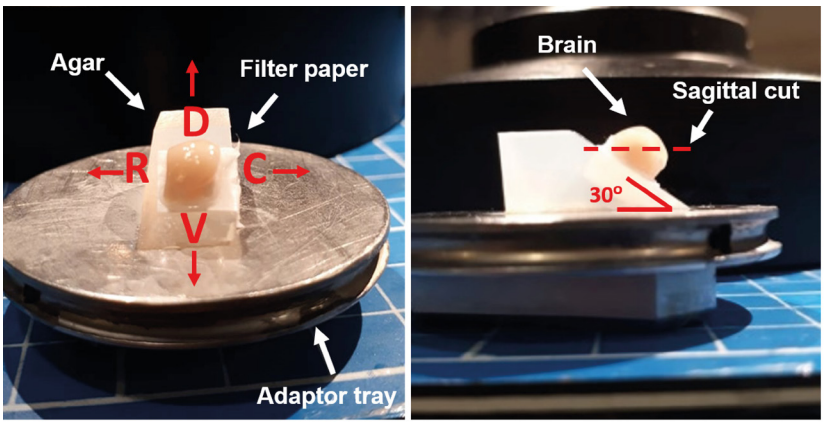

Figure 4. To obtain para-sagittal slices (see sagittal cut, red dotted line), separate the brain hemispheres and glue them by their medial portion at a 30° angle. First, glue the brain to a piece of filter paper and then, glue the filter paper (with the brain) to the agar block (see sagittal slice sequence). The agar block is glue to the adaptor tray (R = rostral, D = dorsal, C = caudal, V = ventral).

2. Once the brain hemisphere is attached to the agar block, place the tissue in an adaptor tray submerged in ice-cold aCSF bubbled with carbogen. To obtain the parasagittal slices of the hippocampal formation (350-400 µm thick), couple the tray to a vibratome. Cut slices (dorsoventrally), and ventral slices containing hippocampus, 4-6 slices from each hemisphere (Figure 5). Immediately, transfer them into a nest beaker and incubate them for 1 h, at room temperature, with bubbled aCSF (Figure 6).

Please cite this article as: Mondragón-Rodríguez *et. al.*, (2020). Hippocampal Unicellular Recordings and Hippocampal-dependent Innate Behaviors in an Adolescent Mouse Model of Alzheimer's disease,*Bio-protocol* 10 (4): e3529. DOI: 10.21769/BioProtoc.3529.

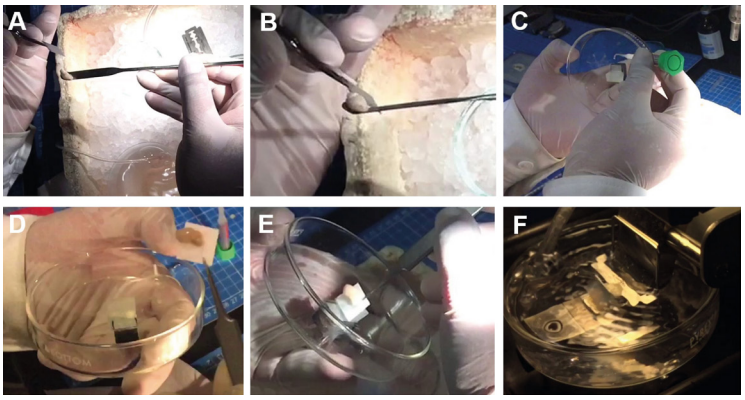

Figure 5. Sagittal slice sequence. With the razor blade, separate the brain hemispheres (A), glue the brain to a piece of filter paper (B) and then, glue the filter paper (with the brain) to the agar block (C to E). Finally, transfer the plate into the slicing chamber of the vibratome and lower the blade holder (F). Once the slice is freed, transfer it to the nest beaker with recovery aCSF.

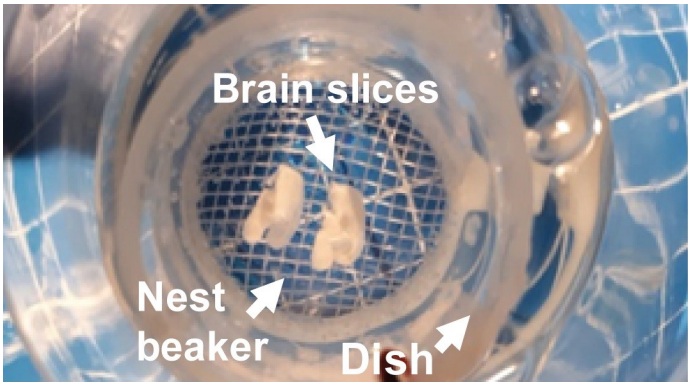

Figure 6. Incubate sagittal slices in aCSF bubbled with carbogen at room temperature for at least one hour for recovery. The nest beaker could be prepared according to Papouin *et al.*, 2018.

3. After recovery, transfer the slices to the recording chamber located in a microscope equipped with optical components to perform Differential Interference Contrast (DIC) (Eclipse E600FN; Nikon, Melville, NY, Figure 7).

Please cite this article as: Mondragón-Rodríguez *et. al.*, (2020). Hippocampal Unicellular Recordings and Hippocampal-dependent Innate Behaviors in an Adolescent Mouse Model of Alzheimer's disease,*Bio-protocol* 10 (4): e3529. DOI: 10.21769/BioProtoc.3529.

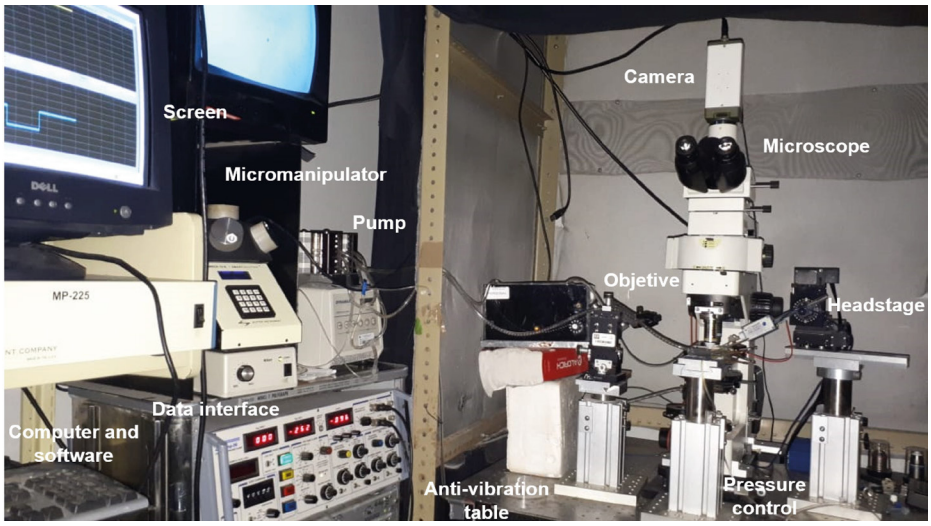

Figure 7. Electrophysiology whole-cell patch-clamp set up and microscope

4. In the recording chamber (Figures 8 and 9), place the slice in a well, which could contain up to 3 ml circulating aCSF bubbled with carbogen, at a temperature of 32 ± 0.5 °C. A total of 30 ml of aCSF continuously recirculate through the recording chamber at a flow rate of 17-20 ml/min (Figures 8 and 9).

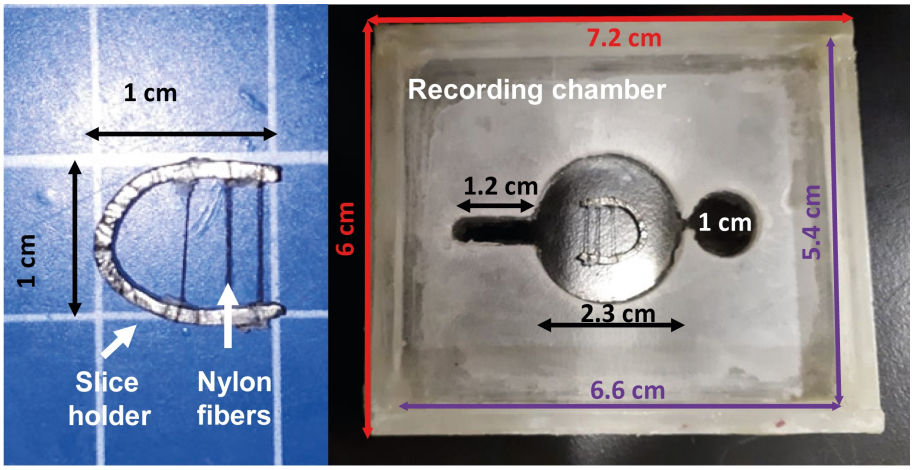

Figure 8. Slice holder and recording chamber. The slice holder is made of a bent and flattened stainless-steel wire crossed by horizontal nylon fibers (around 3 mm apart). The recording chamber is made of acrylic (measuring length in centimeters, cm).

Please cite this article as: Mondragón-Rodríguez *et. al.*, (2020). Hippocampal Unicellular Recordings and Hippocampal-dependent Innate Behaviors in an Adolescent Mouse Model of Alzheimer's disease,*Bio-protocol* 10 (4): e3529. DOI: 10.21769/BioProtoc.3529.

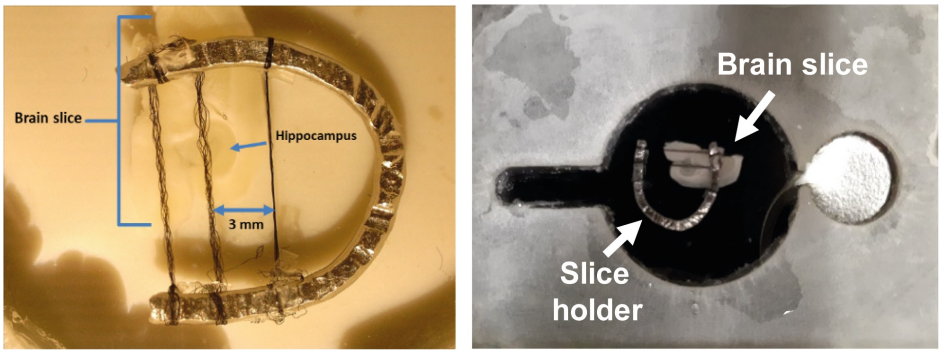

Figure 9. Mounting and holding the brain slice containing the hippocampus onto the recording chamber. The brain slice containing the hippocampal formation is placed onto the recording chamber and immobilized with the holder, leaving the recording area free for electrode location but fixed to maintain stable recording while the slice is perfused at high speed (17-20 ml/min).

5. Perform recordings with glass pipettes (Warner Instruments, G150F-4; Handem, CT) made in a P-97 puller (Sutter Instruments, Novato, CA). The electrode resistance is 2-5 MΩ. Fill pipettes with an internal solution.
6. The visual patch-clamp technique is on the whole-cell configuration in the current clamp mode (Figure 10). The biological signals are measured through an Axoclamp 2B amplifier (Axon Instruments, Foster City, CA). Always focus recordings on neurons located in the CA1 pyramidal area (CA1 has the least heterogeneous neuronal population and the pyramidal cells are arranged into well-defined layers, see Mondragón-Rodríguez *et al.*, 2018a). Once the whole-cell configuration is achieved, hyperpolarizing and depolarizing current pulses are applied to evaluate the intrinsic properties of the recorded neurons (Figures 10 and 11). During this current injection protocol, the neurons remained at the original resting potential (variable between neurons). However, the same protocol was repeated while the cells had a -70 mV membrane potential, which was achieved mostly by applying hyperpolarizing current (for whole-cell patch-clamp video see Sunstrum and Inoue, 2019).

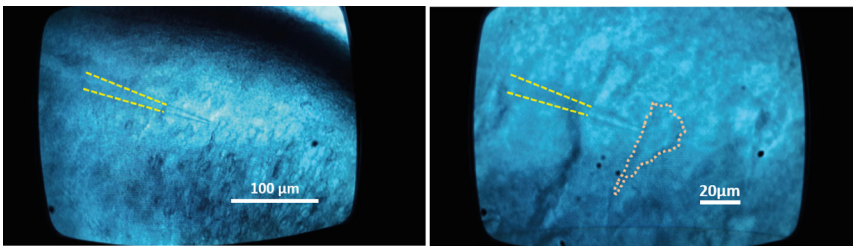

Figure 10. Images of the CA1 pyramidal cell layer visualized through a differential interference contrast (DIC) microscope. The visual patch-clamp technique, in the whole-cell configuration, is achieved with pipette electrodes (highlighted with the dotted line) located on the cell's soma (10x and 40x magnification on the left and right, respectively).

Please cite this article as: Mondragón-Rodríguez *et. al.*, (2020). Hippocampal Unicellular Recordings and Hippocampal-dependent Innate Behaviors in an Adolescent Mouse Model of Alzheimer's disease,*Bio-protocol* 10 (4): e3529. DOI: 10.21769/BioProtoc.3529.

Electrophysiological variables

1. Resting membrane potential (trans-membrane voltage, Vm) is measured immediately after obtaining the whole-cell configuration.
2. Fire frequency is measured as the number of action potentials (APs) generated by a neuron during a supra-threshold pulse of a one-second depolarizing current (Figure 11). To compare all neurons, the minimal depolarizing current injection required to evoke at least one AP (rheobase) is multiplied by two to quantify the frequency of the AP evoked by current injection.
3. Fire frequency adaptation is calculated by dividing T2/T1, where T2 is the time between the last two APs of a train and T1 is the time elapsed between the first two APs of the same train. A value larger than one indicates adaptation of AP firing, whereas a value close to or less than one indicates no adaptation of AP firing or acceleration.
4. Membrane resistance is measured using Ohm's law by dividing the change in voltage induced by the injected current. This measurement is performed for five hyperpolarizing current pulses.

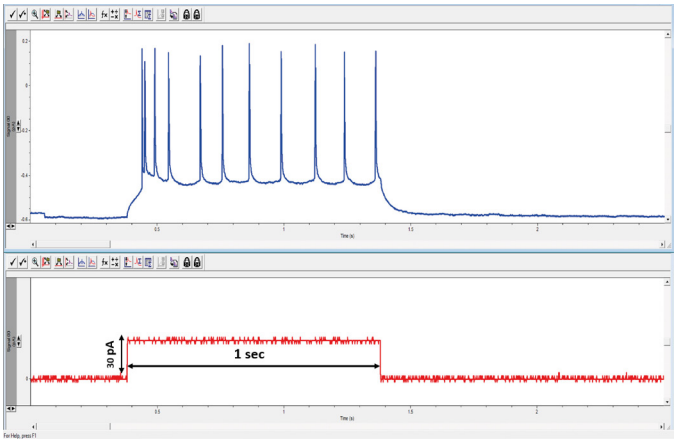

Figure 11. Characterization of the evoked firing pattern of a recorded whole-cell neuron. Injecting a one-second, 30 pA depolarizing current pulse (lower trace) induced a train of action potentials (upper trace), which exhibit the adaptation phenomenon (reduction in firing frequency during steady stimulation).

Subthreshold oscillations

To characterize subthreshold oscillations, bring the membrane potential to the level just below the threshold to trigger APs (although sporadic potential can be induced). Keep the membrane potential at the value at which maximal amplitude subthreshold oscillations could be observed while triggering the least amount of APs as possible. Such voltage is represented in Figure 12.

Please cite this article as: Mondragón-Rodríguez *et. al.*, (2020). Hippocampal Unicellular Recordings and Hippocampal-dependent Innate Behaviors in an Adolescent Mouse Model of Alzheimer's disease,*Bio-protocol* 10 (4): e3529. DOI: 10.21769/BioProtoc.3529.

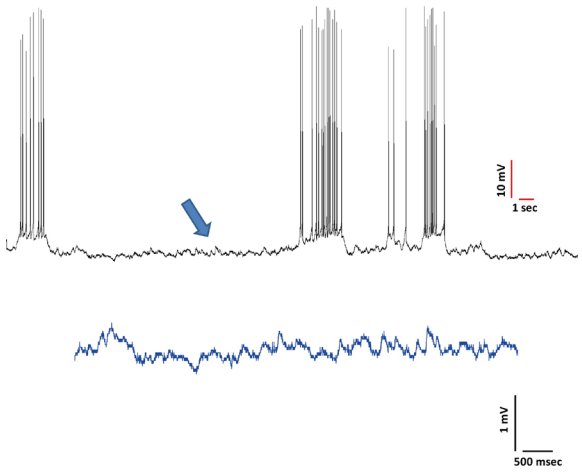

Figure 12. Bring the membrane potential to the level just below the level where action potentials are triggered (see arrow)

Data analysis

A. Behavioral task

Nesting

Take images and evaluate the construction of the nest. Three categories are defined based on those proposed by Deacon (2012), exemplified next:

Assign category 1 when the nestlet is not noticeably made (Figure 13A, >90% intact cotton). Assign category 2 when the nestlet is partially torn up (50 to 90 % of the cotton was shredded), with or without identifiable nesting (Figure 13B). Assign category 3 when a (near) perfect, crater-shaped nest is formed with walls higher than the mouse's body weight, allowing the animal to curl up in the nest with more than 50% of its circumference (Figure 13C, >90% shredded cotton). In sum, the quantification will show the nest rating from 1 to 3, depending on the category (Figure 13).

Note: In a blind experiment, genotypes of all animals are withheld (masked) until the experiments are complete.

Please cite this article as: Mondragón-Rodríguez *et. al.*, (2020). Hippocampal Unicellular Recordings and Hippocampal-dependent Innate Behaviors in an Adolescent Mouse Model of Alzheimer's disease,*Bio-protocol* 10 (4): e3529. DOI: 10.21769/BioProtoc.3529.

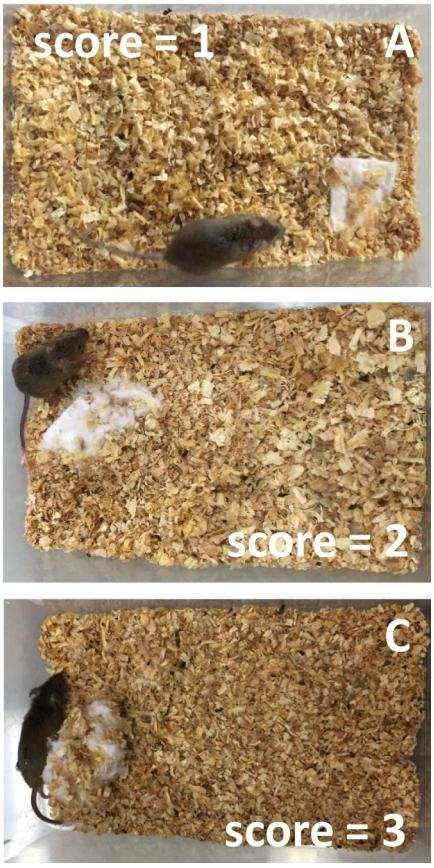

Figure 13. Nestlet is not noticeably made (A, see cotton square), nestlet partially torn up (B, see cotton square) and a near perfect nest (C, see cotton square)

Burrowing

Quantify the weight of displaced pellets (g) after 2 h and then, after 12 h (see Figure 3).

B. Electrophysiology

Patch-clamp

Record with a sampling frequency of 9 KHz. An HS-2 head stage, with a gain of 0.01 MU is used (Molecular Devices). Sample the signals by an analog-digital card coupled to a BNC-2110 connector (National Instruments) to convert the biological (analog) signal into a digital signal. Monitor the recorded signals online with an acquisition software instrument (LabView environment, National Instruments, Austin, TX) and store them in a computer for later analysis.

Analyze the recordings off-line. It is important to mention that we always recorded one slice per animal or one neuron per slice. For classical power spectrum analysis of the membrane potential, segments of five seconds are analyzed using a Fast Fourier Transform algorithm with a Hamming window in Clampfit (Molecular Devices, Figure 14). The power spectrum, from 1 to 60 Hz, is integrated and normalized to control, meaning that the control power spectrum is integrated, and this value is arbitrarily set as 100%.

Please cite this article as: Mondragón-Rodríguez *et. al.*, (2020). Hippocampal Unicellular Recordings and Hippocampal-dependent Innate Behaviors in an Adolescent Mouse Model of Alzheimer's disease,*Bio-protocol* 10 (4): e3529. DOI: 10.21769/BioProtoc.3529.

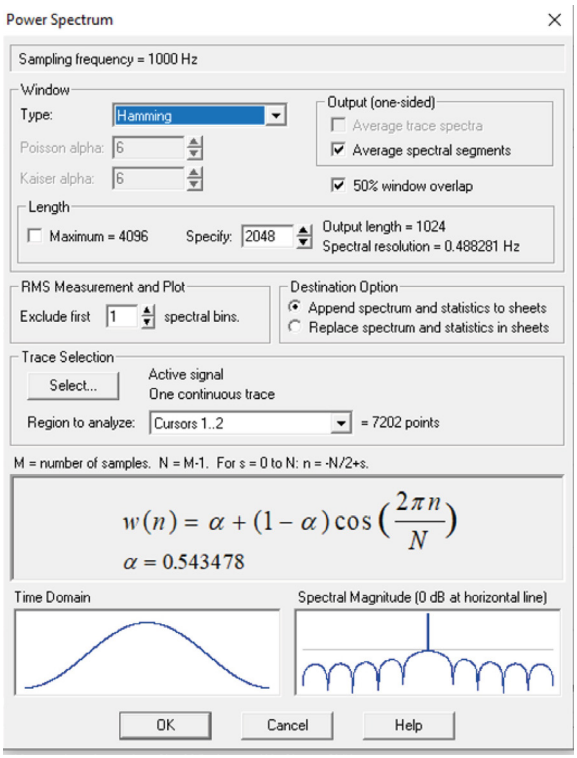

Figure 14. For power spectrum analysis of the membrane potential, analyze segments using a Fast Fourier Transform algorithm with a Hamming window in Clampfit

Expected results

For expected results see Orta-Salazar *et al.*, 2013 and Mondragón-Rodríguez *et al.*, 2018a.

Recipes

1. Intracellular solution for patch-clamp recordings
   140 mM potassium gluconic acid
   10 mM EGTA
   2 mM $MgCl_2$
   10 mM HEPES
   2 mM Na_2ATP
   2 mM LiGTP
   pH 7.4
2. External solution (artificial cerebrospinal fluid (aCSF))
   119 mM NaCl
   3 mM KCl
   1.5 mM $CaCl_2$
   1 mM $MgCl_2$
   25 mM $NaHCO_3$
   30 mM D-glucose

pH 7.4

3. Internal solution
   140 mM potassium gluconic acid
   1 mM $CaCl_2$
   10 mM EGTA
   2 mM $MgCl_2$
   4 mM Na_2ATP
   4 mM LiGTP
   10 mM HEPES
   pH 7.4

Acknowledgments

We thank Jessica Gonzalez Norris for proofreading and Ignacio Martínez García for technical support. This research was supported by the Dirección General de Asuntos del Personal Académico (DGAPA; Grant IN202018 and IN204519) and by CONACYT (Grants; 269021 and A1-S-7540). National Institute of Minority Health and Health Disparities Grant G12MD007591 from the National Institutes of Health and by the Semmes Foundation. S M-R was awarded a Cátedra position from CONACYT, México. This protocol was adapted or modified from Peña *et al.* (2010) and Deacon *et al.* (2012).

Competing interests

The authors declare no competing financial interests.

Ethics

Experimental procedures were approved by the Bioethics Committee of the Institute of Neurobiology, UNAM, Mexico. Approval ID-091/2015-2018.

References

1. Deacon, R. (2012). Assessing burrowing, nest construction, and hoarding in mice. *J Vis Exp*(59): e2607.
2. Deacon, R. M., Raley, J. M., Perry, V. H. and Rawlins, J. N. (2001). Burrowing into prion disease. *Neuroreport* 12(9): 2053-2057.
3. Gjendal, K., Ottesen, J. L., Olsson, I. A. S. and Sørensen, D. B. (2019). Burrowing and nest building activity in mice after exposure to grid floor, isoflurane or ip injections. *Physiol Behav* 206: 59-66.

4. Hashimoto, S and Saido, T. C. (2018). Critical review: involvement of endoplasmic reticulum stress in the aetiology of Alzheimer's disease. *Open Biol*. 8(4): 180024.
5. Ittner, L. M., Ke, Y. D., Delerue, F., Bi, M., Gladbach, A., van Eersel, J., Wolfing, H., Chieng, B. C., Christie, M. J., Napier, I. A., Eckert, A., Staufenbiel, M., Hardeman, E. and Gotz, J. (2010). Dendritic function of tau mediates amyloid-beta toxicity in Alzheimer's disease mouse models. *Cell* 142(3): 387-397.
6. LaFerla, F. M., Green, K. N. and Oddo, S. (2007). Intracellular amyloid-beta in Alzheimer's disease. *Nat Rev Neurosci* 8(7): 499-509.
7. Lilamand, M., Cesari, M., Cantet, C. and Andrieu, S. (2019). Relationship between brain amyloid deposition and instrumental activities of daily living in older individuals: two analyses from the MAPT study. *Geriatr Psychol Neuropsychiatr Vieil* 17(2): 211-220.
8. Mahar, I., Albuquerque, M. S., Mondragon-Rodriguez, S., Cavanagh, C., Davoli, M. A., Chabot, J. G., Williams, S., Mechawar, N., Quirion, R. and Krantic, S. (2017). Phenotypic alterations in hippocampal NPY- and PV-expressing interneurons in a presymptomatic transgenic mouse model of Alzheimer's disease. *Front Aging Neurosci* 8: 327.
9. Mondragón-Rodríguez, S., Gu, N., Fasano, C., Peña-Ortega, F. and Williams, S. (2019). Functional connectivity between hippocampus and lateral septum is affected in very young Alzheimer's transgenic mouse model. *Neuroscience* 401: 96-105.
10. Mondragón-Rodríguez, S., Gu, N., Manseau, F. and Williams, S. (2018b). Alzheimer's transgenic model is characterized by very early brain network alterations and beta-ctf fragment accumulation: reversal by beta-secretase inhibition. *Front Cell Neurosci* 12: 121.
11. Mondragón-Rodríguez, S., Perry, G., Luna-Muñoz, J., Acevedo-Aquino, M. C. and Williams, S. (2014). Phosphorylation of tau protein at sites Ser (396-404) is one of the earliest events in Alzheimer's disease and Down syndrome. *Neuropathol Appl Neurobiol* 40(2): 121-135.
12. Mondragón-Rodríguez, S., Perry, G., Peña-Ortega, F. and Williams, S. (2017). Tau, amyloid beta and deep brain stimulation: aiming to restore cognitive deficit in Alzheimer's disease. *Curr Alzheimer Res* 14(1): 40-46.
13. Mondragón-Rodríguez, S., Perry, G., Zhu, X., Moreira, P. I., Acevedo-Aquino, M. C. and Williams, S. (2013). Phosphorylation of tau protein as the link between oxidative stress, mitochondrial dysfunction, and connectivity failure: implications for Alzheimer's disease. *Oxid Med Cell Longev* 2013: 940603.
14. Mondragón-Rodríguez, S., Salas-Gallardo, A., González-Pereyra, P., Macías, M., Ordaz, B., Peña-Ortega, F., Aguilar-Vazquez, A., Orta-Salazar, E., Diaz-Cintra, S., Perry, G. and Williams, S. (2018a). Phosphorylation of Tau protein correlates with changes in hippocampal theta oscillations and reduces hippocampal excitability in Alzheimer's model. *J Biol Chem* 293(22): 8462-8472.
15. Mucke, L. and Selkoe, D. J. (2012). Neurotoxicity of amyloid beta-protein: synaptic and network dysfunction. *Cold Spring Harb Perspect Med* 2(7): a006338.

16. Oddo, S., Caccamo, A., Kitazawa, M., Tseng, B. P. and LaFerla, F. M. (2003). Amyloid deposition precedes tangle formation in a triple transgenic model of Alzheimer's disease. *Neurobiol Aging* 24(8): 1063-1070.
17. Orta-Salazar, E., Feria-Velasco, A., Medina-Aguirre, G. I. and Díaz-Cintra, S. (2013). Morphological analysis of the hippocampal region associated with an innate behaviour task in the transgenic mouse model (3xTg-AD) for Alzheimer disease. *Neurologia* 28(8): 497-502.
18. Papouin, T and Haydon, P. G. (2018). Obtaining Acute Brain Slices. *Bio-protocol* 8(2): e2699.
19. Peña, F., Ordaz, B., Balleza-Tapia, H., Bernal-Pedraza, R., Marquez-Ramos, A., Carmona-Aparicio, L. and Giordano, M. (2010). Beta-amyloid protein (25-35) disrupts hippocampal network activity: role of Fyn-kinase. *Hippocampus* 20(1): 78-96.
20. Peña-Ortega, F., Solis-Cisneros, A., Ordaz, B., Balleza-Tapia, H. and Javier Lopez-Guerrero, J. (2012). Amyloid beta 1-42 inhibits entorhinal cortex activity in the beta-gamma range: role of GSK-3. *Curr Alzheimer Res* 9(7): 857-863.
21. Salgado-Puga, K., Prado-Alcalá, R. A. and Peña-Ortega, F. (2015). Amyloid β enhances typical rodent behavior while it impairs contextual memory consolidation. *Behav Neurol* 2015: 526912.
22. Selkoe, D. J. (1990). Deciphering Alzheimer's disease: the amyloid precursor protein yields new clues. *Science* 248(4959): 1058-1060.
23. Sunstrum, J. K. and Inoue, W. (2019). Evaluation of Synaptic Multiplicity Using Whole-cell Patch-clamp Electrophysiology. *J Vis Exp* 146.
24. Tong, B. C., Wu, A. J., Li, M. and Cheung, K. H. (2018). Calcium signaling in Alzheimer's disease & therapies. *Biochim Biophys Acta Mol Cell Res* 1865(11 Pt B): 1745-1760.
25. V-Ghaffari, B., Kouhnavard, M. and Kitajima, T. (2016). Biophysical properties of subthreshold resonance oscillations and subthreshold membrane oscillations in neurons. *J Biol Syst* 24(4): 561-575.

